Struct Chem
DOI 10.1007/s11224-013-0223-3

ORIGINAL RESEARCH

Mechanistic investigation and DFT calculation of the new reaction between *S*-methylisothiosemicarbazide and methyl acetoacetate

Violeta Marković · Svetlana Marković · Ana Janićijević · Marko V. Rodić · Vukadin M. Leovac · Nina Todorović · Snežana Trifunović · Milan D. Joksović

Received: 6 December 2012 / Accepted: 28 January 2013

Abstract A study on the synthesis and mechanistical aspects of formation of 3-methyl-5-oxo-3-pyrazolin-1-carboxamide (MOPC) starting from *S*-methylisothiosemicarbazide hydrogen iodide and methyl acetoacetate was performed. In the alkaline aqueous solution, the intermediate methyl acetoacetate *S*-methylisothiosemicarbazone undergoes substitution of CH_3S^- anion by hydroxide anion, cyclization, carbanion formation, and elimination of methanol, thus yielding corresponding Na-enolate salt of pyrazol-5-one derivative. The structure of the compound obtained after protonation of the formed enolate salt was determined by means of spectroscopic techniques and single-crystal X-ray diffraction analysis. The mechanism of conversion of methyl acetoacetate *S*-methylisothiosemicarbazone into MOPC was investigated by means of the B3LYP functional, and it was found that the reaction is thermodynamically controlled.

Keywords Pyrazolone · Reaction mechanism · DFT · Thermodynamic and kinetic control

Electronic supplementary material The online version of this article (doi:10.1007/s11224-013-0223-3) contains supplementary material, which is available to authorized users.

V. Marković · S. Marković · A. Janićijević · M. D. Joksović (✉)
Department of Chemistry, Faculty of Science, University of Kragujevac, R. Domanovica 12, 34000 Kragujevac, Serbia
e-mail: mjoksovic@kg.ac.rs

M. V. Rodić · V. M. Leovac
Department of Chemistry Biochemistry and Environmental Protection, Faculty of Science, University of Novi Sad, Trg D. Obradovića 3, 21000 Novi Sad, Serbia

N. Todorović
Institute for Chemistry, Technology and Metallurgy, Njegoševa 12, 11000 Belgrade, Serbia

S. Trifunović
Faculty of Chemistry, University of Belgrade, Studentski trg 16, P.O. Box 158, 11000 Belgrade, Serbia

Introduction

Pyrazolones represent an important class of heterocyclic compounds with a wide range of applications in both chemistry and biology due to their favorable pharmacological properties. These characteristics caused an increasing interest of medicinal chemists for this research area in the last decades. For example, antipyrine (2,3-dimethyl-1-phenylpyrazol-5-one) and its analogs aminopyrine, dipyrone and propyphenazone are known for a long time as antipyretic, analgesic, and anti-inflammatory substances [1, 2]. A new pyrazol-5-one compound, edaravone (3-methyl-1-phenyl-2-pyrazoline-5-one, Radicut®, Mitsubishi Tanabe Pharma Corporation) has been presented as a strong free radical scavenger and a promising drug for the treatment of brain ischemia [3]. A number of other pyrazolone compounds have been synthesized and found to exhibit diverse biologic and pharmacological properties [4–7].

The synthesis of carboxamide derivatives of pyrazolones starting from β-keto esters and semicarbazide hydrochloride is the known way of preparation of this class of compounds [8]. The study by microwave irradiation was carried out to investigate the possibility of performing this reaction without use of any solvent and in much shorter reaction time [9].

The reaction mechanism of the known synthesis of 3-methyl-5-oxo-3-pyrazolin-1-carboxamide (MOPC, **1**) occurs by initial regioselective attack of the least hindered and more nucleophilic nitrogen atom of the semicarbazide hydrazine

Published online: 08 February 2013

moiety on the ketone carbon atom of the β-keto ester (Scheme 1) [10]. This claim is supported by identification of the corresponding hydrazone intermediate. The regioselectivity of the reaction is also a result of higher reactivity of ketone moiety over ester [11]. The next step is an intramolecular cyclization between the ester group and the second nitrogen atom of hydrazine moiety to provide an equilibrium mixture of the tautomeric forms of the compound **1**.

The reaction of *S*-alkylated isothiosemicarbazides with ketone compounds proceeds in analogy with the reaction of hydrazine derivatives giving *S*-alkylated thiosemicarbazones. In our previous research reaction, acetylacetone and *S*-methylisothiosemicarbazide hydrogen iodide unexpectedly yielded 3-aminopyrazole derivative in an alkaline medium [12]. Mechanism of the formation of this compound was examined by means of NMR studies and DFT calculations. A cyclic intermediate 5-hydroxy-3,5-dimethyl-1-*S*-methylisothiocarbamoyl-2-pyrazolinium iodide was formed instead of acetylacetone mono-*S*-methylisothiosemicarbazone. In alkaline medium, it is subjected to ring opening reaction forming the keto–imine form of acetylacetone mono-*S*-methylisothiosemicarbazone. Herein, as a continuation of the previous work, we have focused our attention on performing a reaction between *S*-methylisothiosemicarbazide hydrogen iodide and methyl acetoacetate. Unlike the former, this reaction resulted in the formation of 3-methyl-5-oxo-3-pyrazolin-1-carboxamide (MOPC). In this paper, we present a study on the synthesis and mechanistical aspects of formation of this pyrazol-5-one derivative.

Results and discussion

Synthesis of 3-methyl-5-oxo-3-pyrazolin-1-carboxamide (MOPC, 1)

The precursor methyl acetoacetate *S*-methylisothiosemicarbazone (**2b**) was formed by refluxing of the equimolar amounts of methyl acetoacetate and *S*-methylisothiosemicarbazide hydrogen iodide in ethanol during 1 h. It is also possible to synthesize this compound with a higher degree of purity if the mixture is left standing for 48 h upon 1 h of stirring at the room temperature. The absence of an AB system in its ^{1}H NMR spectrum for methylene protons excludes the existence of the cyclic form. After the solvent was evaporated, water was poured into the residue and the granulated NaOH was added to the stirring mixture. Compound **2b** is sensitive to hydrolysis in water which results in the significant formation of starting reactants as established by analyzing of ^{1}H NMR spectrum in D_2O after 1 h of standing. Therefore, it is necessary to add NaOH immediately after addition of water. Owing to the dissolving of NaOH in water, the reaction mixture becomes hot. Attempts to cool the flask led to the decrease of the reaction yield, implying that this cyclization reaction is very slow at the room temperature. The use of granulated NaOH enabled slower dissolving and therefore prolongation of heat evolving. Molar ratio of NaOH to **2b** of 11:1 appeared to be the most effective. Lower molar ratio resulted in prolongation of the reaction time and decrease of the yield of enolate salt **16**. As for concentration, 35–40 % aqueous solution of NaOH gave the best results (Scheme 2).

The high purity of **16**, formed few minutes upon the addition of NaOH, does not require further purification. Treatment of the enolate salt **16** (yield: 54 % relative to *S*-methylisothiosemicarbazide hydrogen iodide) with 2 M HCl resulted in the formation of the corresponding protonated form which instantly underlies tautomerisation to 3-methyl-5-oxo-3-pyrazolin-1-carboxamide (MOPC, **1**, 75 % yield relative to **16**).

2D NMR study

The structural confirmation of MOPC (**1**) was based on elemental analysis, HRMS, one-dimensional (1D) and 2D NMR techniques, and X-ray diffraction analysis. Detailed assignation of NMR data is performed by means of ^{1}H, ^{13}C,

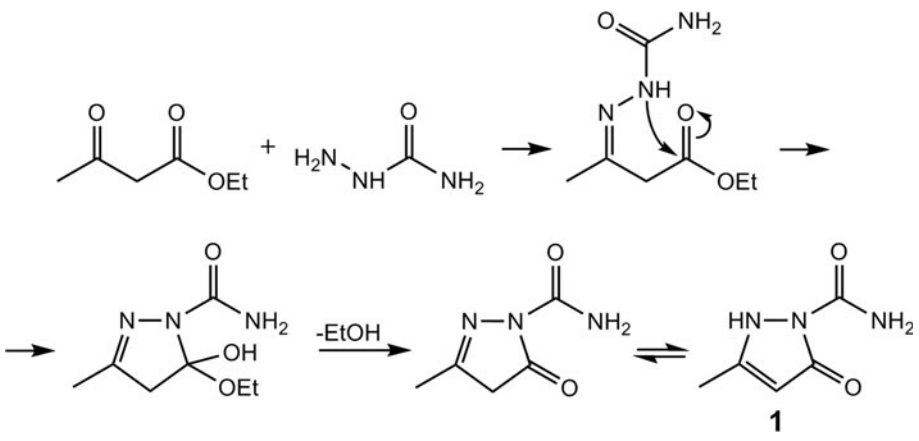

Scheme 1 Mechanism of formation of 3-methyl-5-oxo-3-pyrazolin-1-carboxamide (MOPC, **1**) from ethyl acetoacetate and semicarbazide

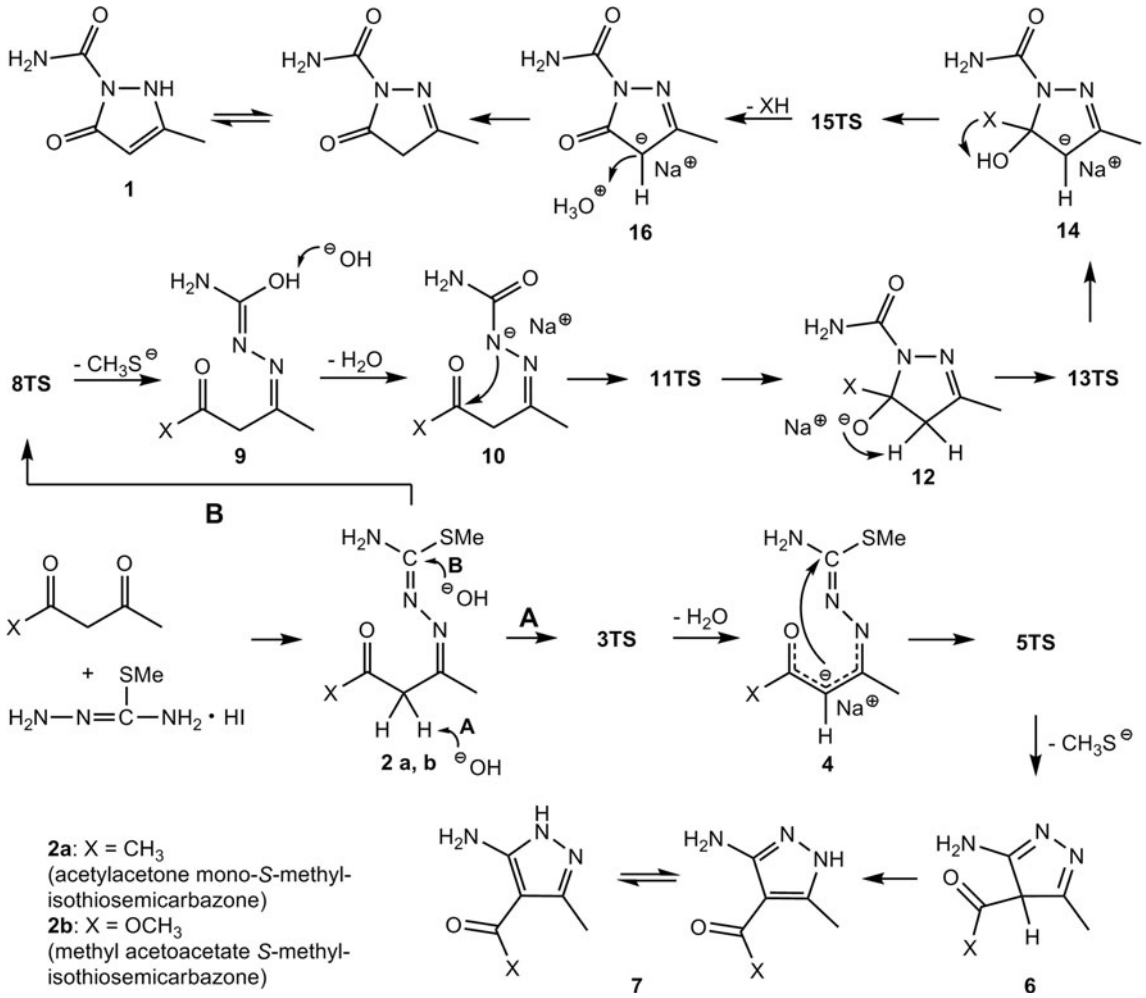

Scheme 2 Two different mechanistic pathways **A** and **B** for the compounds **2a** and **b**. Mechanism **A**: formation of a 3-aminopyrazole (**7**) from **2a** (operative mechanism [12]); there is no reaction from **2b** according to this mechanism. Mechanism **B**: formation of MOPC (**1**) from **2b** (operative mechanism, present work); there is no reaction from **2a** according to this mechanism

DEPT, HSQC, HMBC, NOESY, $^{1}H–^{15}N$ HSQC, and $^{1}H–^{15}N$ HMBC spectra (Figs. S1–S10, Supplementary data).

The position of the methyl group at 11.89 ppm can be easily established according to correlations in HSQC spectrum. In addition, NOESY spectrum displays a cross peak between methyl protons and proton at C4. On the other hand, HMBC spectrum shows two- and three-bond correlations of methyl protons with C3 and C4, respectively. The proton at C4 gives two two-bond cross peaks, one with C3 atom and the other with the carbon atom of the carbonyl group of the pyrazolone ring.

The assignation of the NH_2 nitrogen atom was performed according to the $^{1}H–^{15}N$ HSQC spectrum which depicts a correlation of signals at 7.68 and 8.34 ppm with nitrogen atom at −297.4 ppm. This implies that protons are bonded to the same nitrogen atom: in this case, NH_2 group of the carboxamide moiety.

The absence of the expected correlation of N2–H can be explained with the existence of annular tautomerism as well as a high degree of tautomerisability of this nitrogen atom. Indeed, after 2 weeks of standing in DMSO-d_6 solution, NMR spectra became more complex and four additional signals in ^{1}H NMR attributed to methyl protons were observed. Furthermore, NOESY spectrum reveals an off-diagonal cross peak of N2–H with water present in the deutero solvent. On the other hand, $^{1}H–^{15}N$ HMBC spectrum shows a correlation between methyl protons and nitrogen atom at −233.3 ppm, which can only be assignated to N2 atom. N1 atom at −193.7 ppm exhibits two three-bond correlations with the proton at C4 and with one of NH_2 protons. The absence of correlation with the other NH_2 proton can be explained by the contribution of free electron pair of this nitrogen atom to the resonance of the amide group.

Crystallographic study

Molecular structures of the MOPC and atomic labeling scheme are given in Fig. 1, while structural parameters are listed in Tables S1, S2, and S3 (Supplementary data).

The molecule is highly planar and displacement from mean plane for non-hydrogen atoms are in range 0.001 (2) to 0.040 (1) Å with N1 atom deviating the most. Delocalization of electron density is evident in pyrazole ring with bond lengths between those characteristic for pure single or double bonds due to sp^2 hybridization of atoms. Formal double bond between Csp^2–Csp^2 can be ascribed to C3–C4 distance, while other formally correspond to single bonds [13, 14]. In order to corroborate that the main tautomer in the solid state is MOPC, bond lengths within pyrazole ring are compared with those found in other 3-methyl-5-oxo-3-pyrazoline-*N*(1)-substituted derivatives [15–22], and results are listed in Table 1. All bond lengths are in good agreement with those found in structurally related compounds, as N1–N2, N1–C5, C5–C4, C4–C3, and C3–N2 distances in MOPC (1.368 (2), 1.400 (2), 1.407 (2), 1.367 (2), and 1.334 (2) Å, respectively) deviate not more than ±0.01 Å from the average values calculated from literature data (1.38, 1.40, 1.41, 1.36, and 1.34 Å, respectively).

Carboxamide group is coplanar with the pyrazole ring with dihedral angle between N1/N2/C3/C4/C5 and O2/C7/N3 being 3.1 (3)°. The *trans* orientation of N3 toward N2 is favored by intermolecular hydrogen bond N3–H3*A*···O1 which results in formation of a six-membered ring with graph-set descriptor *S*(6) [23].

All potential hydrogen bond donors and acceptors are involved in hydrogen bonding. Strong N–H···O hydrogen bonds determine the supramolecular architecture of the MOPC (**1**) molecules, and their geometrical parameters are given in Table S4 (Supplementary data). As expected, amide groups in the crystal form head-to-head amide group homosynthons [24]. Namely, hydrogen bond N3–H3*B*···O2^{i} [symmetry code: (i) $-x+1$, $-y+1$, $-z$] connects two neighboring molecules into centrosymmetric dimer resulting in $R_2^2(8)$ motif [23]. Furthermore, N2–H2···O1^{ii} [symmetry code: (ii) $x-1$, y, z] interaction connects dimers laterally into highly planar 1D pattern, which propagates along direction of *a* axis, as depicted in Fig. 2. This hydrogen bond can serve as additional proof of existence of hydrogen atoms bonded to N2 and correct assignment of tautomeric form of **1**. The arrangement of

Table 1 Comparison of bond lengths (Å) within pyrazole ring of MOPC (**1**) with those found in 3-methyl-5-oxo-3-pyrazoline-*N*(1)-substituted derivatives reported in literature

	N1–N2	N1–C5	C5–C4	C4–C3	C3–N2	References
	1.376 (3)	1.420 (2)	1.408 (4)	1.367 (3)	1.337 (2)	[15]
	1.378 (2)	1.414 (2)	1.412 (3)	1.375 (3)	1.338 (3)	[16]
	1.400 (2)	1.392 (2)	1.425 (2)	1.357 (3)	1.355 (3)	[17]
	1.380 (4)	1.408 (4)	1.403 (6)	1.367 (4)	1.343 (5)	[18]
	1.376 (3)	1.394 (4)	1.412 (5)	1.359 (5)	1.348 (5)	[19]
	1.387 (3)	1.400 (4)	1.418 (5)	1.356 (4)	1.345 (4)	[19][a]
	1.383 (3)	1.413 (4)	1.415 (4)	1.362 (4)	1.334 (4)	[20]
	1.380 (2)	1.379 (2)	1.401 (2)	1.356 (2)	1.340 (2)	[21]
	1.389 (3)	1.390 (4)	1.414 (3)	1.355 (4)	1.350 (4)	[22]
Minimum	1.376 (3)	1.379 (2)	1.401 (2)	1.355 (4)	1.343 (5)	
Maximum	1.400 (2)	1.420 (2)	1.425 (2)	1.375 (3)	1.355 (3)	
Average	1.38	1.40	1.41	1.36	1.34	
MOPC	1.368 (2)	1.400 (2)	1.407 (2)	1.367 (2)	1.334 (2)	[This work]

[a] Asymmetric unit contains two independent molecules

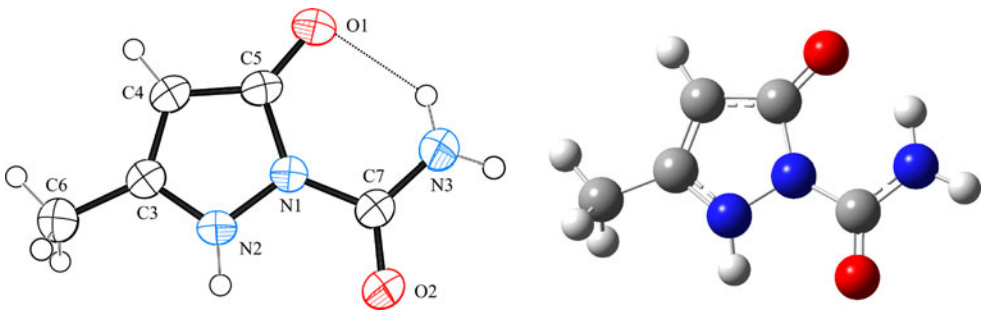

Fig. 1 Molecular structure of MOPC (**1**): experimental (*left*) and calculated (*right*). *Ellipsoids* are drawn at 50 % probability level. Only one orientation of disordered methyl hydrogen atoms is shown with site occupancy factors of 0.5. Calculated geometry corresponds to the solvated molecule

dimers in ribbon results in the hydrogen bonding ring which is described by $R_6^4(18)$ graph. The neighboring ribbons are connected via dipole–dipole interaction between stacked carbonyl groups (Fig. 3). Geometry of this interaction can be classified as sheared antiparallel motif after Allen et al. [25] with O1–C5^{iii} distance 3.184 (2) Å [symmetry code: (iii) $2 - x$, $1 - y$, $1 - z$], and C5–O1···C5^{iii} and O1–C5···O1^{iii} angles 101.5 (1)° and 78.5 (1)°, respectively. Crystal packing is achieved by layering ribbons which leads to high packing index of 71.1 % filled space.

The structure of **1** in the aqueous phase was calculated by the B3LYP/6-311 ++G(d,p) level of theory in combination with the CPCM solvation model (Fig. 1). The experimental and calculated geometrical parameters of **1** are presented in Tables S1, S2, and S3. Obviously, the differences in geometrical parameters between the experimental and calculated structures of **1** are very small. These differences originate to a large degree from different intermolecular interactions in the crystal (where a molecule of **1** is surrounded with the molecules of the same kind) and aqueous solution (where a molecule of **1** is surrounded with the water molecules). Taking this fact into account, this theoretic model was further employed to elucidate the mechanism of transformation of the precursor **2b** into **1**.

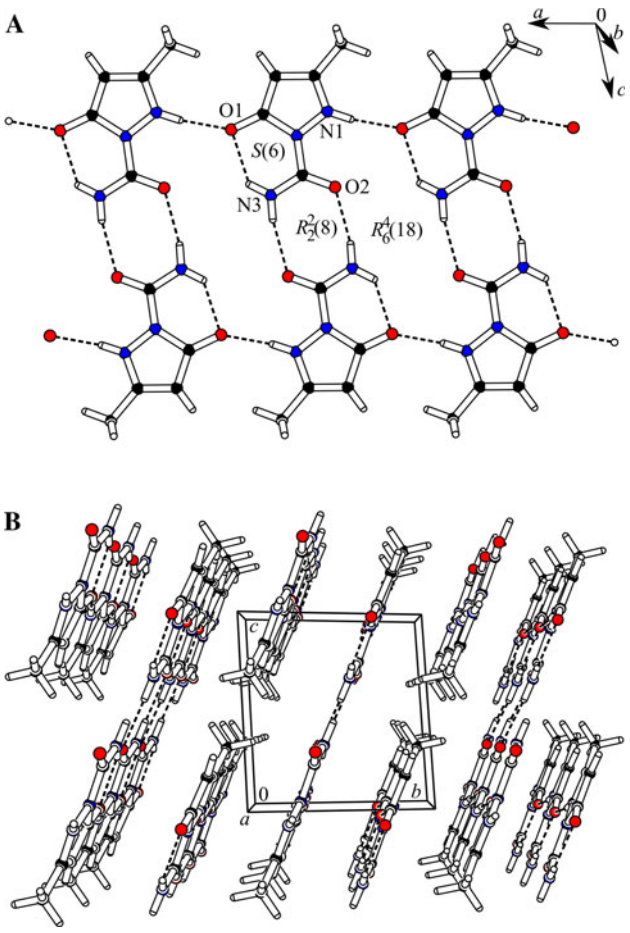

Fig. 2 Supramolecular arrangement of molecules in ribbon via hydrogen bonds (**a**), crystal packing viewed perpendicular to *bc* plane (**b**)

Mechanism of formation of 3-methyl-5-oxo-3-pyrazolin-1-carboxamide

In Scheme 2 according to the mechanism **A**, the keto–imine tautomer **2a** undergoes the further cyclization by carbanionic mechanism forming corresponding 4-acetyl-3(5)-amino-5(3)-methylpyrazole **7** [12]. In order to investigate a possible range of application of mechanism **A**, herein, we performed a reaction between methyl acetoacetate and *S*-methylisothiosemicarbazide hydrogen iodide. According to this mechanism, the expected 3-aminopyrazole derivative would have ester or carboxylic moiety (upon alkaline hydrolysis) at C4 position. Opposite to our expectations, formed intermediate methyl acetoacetate *S*-methylisothiosemicarbazone (**2b** in Scheme 2) in alkaline conditions yielded corresponding Na-enolate salt **16**, which upon the treatment with 2 M HCl formed 3-methyl-5-oxo-3-pyrazolin-1-carboxamide (MOPC, **1**).

Our computational research showed that **2b** can undertake two different pathways in the basic environment. Now, we will consider the mechanism **B** (Scheme 2), which is in accord with the obtained experimental results. The revealed transition states (TSs) are given in Fig. 4, whereas all elementary steps of the reaction are presented in Supplementary data via the optimized geometries of the related participants.

Mechanism **B** begins with nucleophilic attack of OH^- at the electrophilic carbon-bearing CH_3S group (natural bond orbital [NBO] charge = 0.311). This step of the reaction proceeds via transition state **8TS**, where the new C–O bond is being formed, while the C–S bond is being cleaved, implying that the CH_3S^- anion is substituted by the

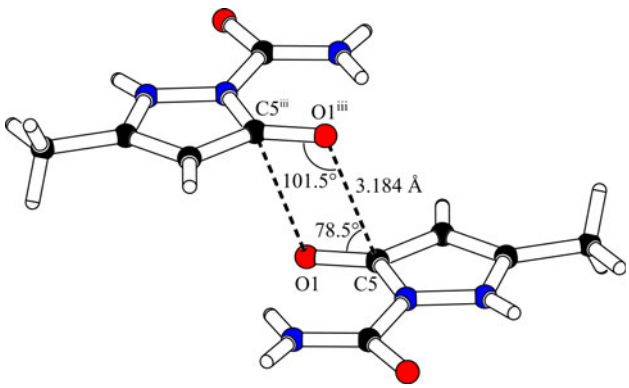

Fig. 3 Dipole–dipole interaction between stacked carbonyl groups. Symmetry code: (iii) $2 - x$, $1 - y$, $1 - z$

hydroxide anion. This substitution leads to the formation of intermediate **9** where hydrogen of hydroxyl group is extremely acidic (NBO charge = 0.513). Thus, OH^- from the alkaline medium performs an abstraction of this proton. This step of the reaction occurs spontaneously with the energetic stabilization of the system, and the formation of intermediate **10**. As expected, in this intermediate nitrogen bears notable negative charge (−0.617), whereas carbonyl carbon is electrophilic (NBO charge = 0.852) allowing an intramolecular nucleophilic attack. The system passes through transition state **11TS**, and the cyclic intermediate **12** is formed in this way. The NBO analysis of **12** revealed single C–O bond in alkoxide. In accordance with this finding, the oxygen bears strong negative charge (−0.916). Thus, intramolecular abstraction of proton from the adjacent methylene group by the alkoxy group is expected. This reaction step takes place via transition state **13TS**, yielding intermediate carbanion **14**. This carbanion further undergoes elimination of CH_3OH, via transition state **15TS**. **15TS** is distinguished by the formation of the O–H bond in methanol and cleavage of the C–O and O–H bonds in intermediate **14** (Fig. 4). These alterations lead to the formation of the carbanion **16**, the existence of which was confirmed by means of NMR spectra. Addition of HCl invokes spontaneous abstraction of proton from hydronium ion, giving the corresponding pyrazolone **1**.

The second path revealed by DFT calculations is mechanism **A** (Scheme 2, for compound **2b**). The structures of the TSs appearing in mechanism **A** are presented in Fig. 5. This mechanism proceeds with the abstraction of proton of the methylene group by OH^-, via transition state **3TS**, leading to the formation of the corresponding carbanion **4**. It further undergoes intramolecular cyclization by nucleophilic attack at the C-atom bearing CH_3S group. In transition state **5TS**, the new C–C bond is being formed, whereas the C–S bond is being cleaved, implying that the CH_3S^- anion is eliminated in this step of the reaction. The so-formed intermediate **6** further undergoes tautomerisation, yielding thermodynamically more favorable tautomeric equilibrium of corresponding 3-aminopyrazoles **7**. However, experimental results show that the reaction does not occur according to this pathway. Keeping in mind this fact, our goal was to find out the explanation by comparing two different mechanisms.

Comparison of mechanisms **A** and **B**

It is clear that acetylacetone mono-*S*-methylisothiosemicarbazone (**2a**) and methyl acetoacetate *S*-methylisothiosemicarbazone (**2b**) conform to two different mechanisms: **A** and **B**. In order to accomplish this challenging task we investigated mechanism **B** starting from acetylacetone mono-*S*-methylisothiosemicarbazone (Supplementary data). Note that mechanism **A** for acetylacetone mono-*S*-methylisothiosemicarbazone has already been investigated and confirmed [12]. In Tables 2 and 3, all relevant relative free energies concerning both mechanisms and both starting compounds, as well as activation enthalpies and entropy terms for operative mechanisms are listed.

Tables 2 and 3 reveal that all elementary steps are enthalpy controlled, but not entropy controlled ($\Delta H_a^{\ddagger} > -T\Delta S_a^{\ddagger}$). This implies that the rates of the reactions are governed more by the bond strengths than by the issues of orientation, trajectory, accessibility, etc. Table 2 shows that the energetics concerning both compounds is very similar. According to mechanism **A,** both reactions are

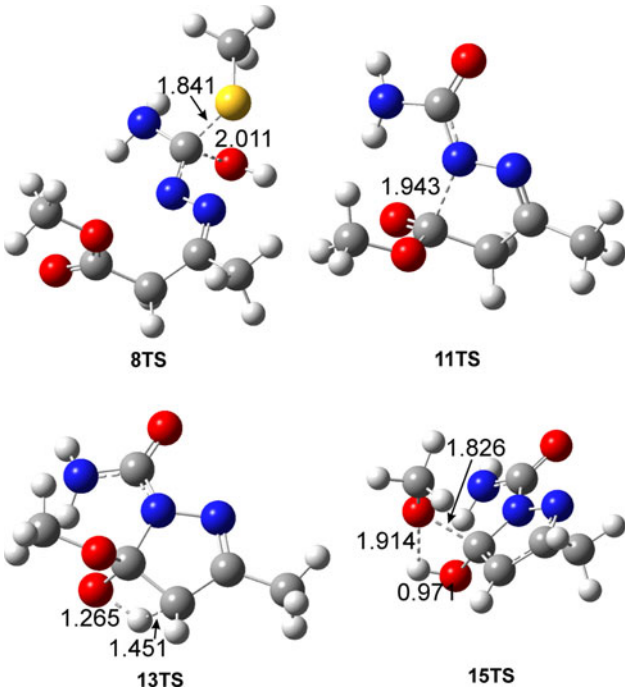

Fig. 4 Optimized geometries of the TSs figuring in mechanism **B** for compound **2b** with crucial intramolecular distances (Å) indicated

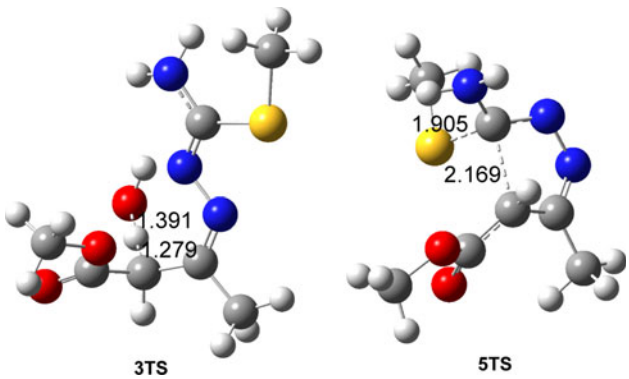

Fig. 5 Optimized geometries of the TSs figuring in mechanism **A** for compound **2b** with crucial intramolecular distances (Å) indicated

Table 2 Activation parameters: enthalpies ($\Delta H_a^{\ddagger}$), entropy terms ($-T\Delta S_a^{\ddagger}$), and free energies ($\Delta G_a^{\ddagger}$); and reaction free energies (ΔG_r) in elementary steps of mechanism **A**

Reaction steps	**2a** [12]				**2b**	
	$\Delta H_a^{\ddagger}$	$-T\Delta S_a^{\ddagger}$	$\Delta G_a^{\ddagger}$	$\Delta G_r^{\ddagger}$	$\Delta G_a^{\ddagger}$	ΔG_r
1. **2a**, **b** + HO^- → **3TS** → **4** + H_2O	4.5	4.3	8.8	−49.4	14.8	−40.3
2. **4** → **5TS** → **6** + CH_3S^-	110.6	5.1	115.7	−72.4	112.0	−75.3
3. Tautomerisation of **6**–**7**				−88.7		−88.8
Overall reaction[a]			66.3	−210.6	71.8	−204.3

All energies are given in kJ/mol

[a] In Tables 2 and 3 $\Delta G_a^{\ddagger}$ values for overall reactions were calculated relative to the corresponding RCs

Table 3 Activation parameters: enthalpies ($\Delta H_a^{\ddagger}$), entropy terms ($-T\Delta S_a^{\ddagger}$), and free energies ($\Delta G_a^{\ddagger}$); and reaction free energies (ΔG_r) in elementary steps of mechanism **B**

Reaction steps	**2a** [12]		**2b**			
	$\Delta G_a^{\ddagger}$	ΔG_r	$\Delta H_a^{\ddagger}$	$-T\Delta S_a^{\ddagger}$	$\Delta G_a^{\ddagger}$	$\Delta G_r^{\ddagger}$
1. **2a**, **b** + HO^- → **8TS** → **9** + CH_3S^-	110.8	63.0	67.9	42.7	110.6	64.3
2. **9** + HO^- → **10** + H_2O		−80.5				−76.2
3. **10** → **11TS** → **12**	18.8	9.9	23.5	9.9	33.4	28.6
4. **12** → **13TS** → **14**	157.7	69.7	185.8	0.3	186.1	88.4
5. **14** → **15TS** → **16** + XH	160.6	−172.0	15.0	1.5	16.5	−211.3
6. **16** + H_3O^+ → **1**		−189.3				−189.3
Overall reaction	222.7	−299.2			202.8	−295.5

All energies are given in kJ/mol

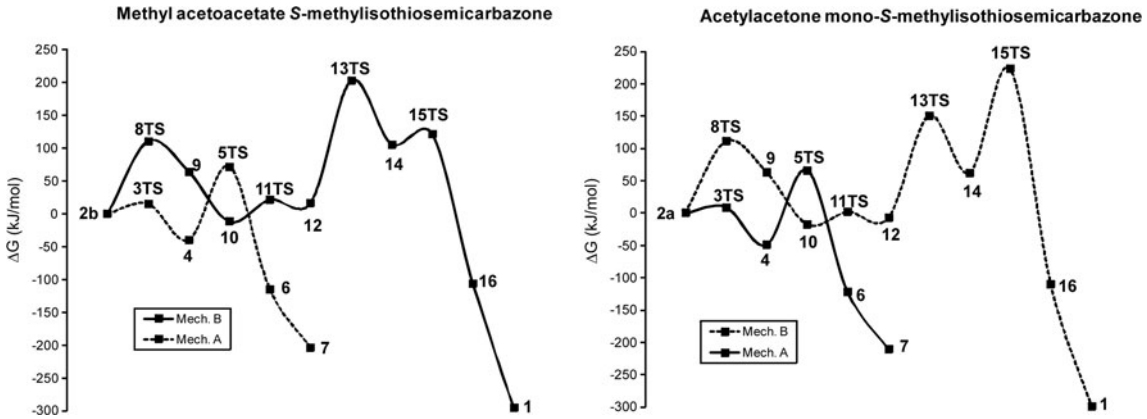

Fig. 6 Energy profiles for mechanisms **A** and **B**. Energies were calculated relative to reactants. *Solid lines* represent operative mechanisms

exothermic and activation energies are moderately low. The rate-determining step is elementary reaction 2. Taking into account that step 1 is exothermic, the $\Delta G_a^{\ddagger}$ values for the overall reactions are rather low. On the other hand, mechanism **B**, in the case of both compounds, requires significantly higher activation energies, whereas the reactions are remarkably exothermic (Table 3). Some reaction steps require significantly different activation barriers. This particularly refers to step 5, where elimination of methanol (for compound **2b**) and methane (for compound **2a**) requires 16.5 and 160.6 kJ/mol, respectively. This difference can be attributed to much higher electronegativity of oxygen over carbon, and to the very unfavorable orientation of the hydrogen of the hydroxyl group in regard to the

carbon of the methyl group in **14** for compound **2a** (Fig. S24; see Fig. S15 for comparison). This hydrogen atom takes such position to avoid the vicinity of partially positively charged hydrogens of the methyl and amino groups. The resulting intramolecular distance of 3.178 Å between the reaction sites induces constrains for the formation of **15TS** (for compound **2a**). Taking into account that step 4 is endothermic, it turns out that the $\Delta G_a^{\ddagger}$ value for the overall reaction of transformation of acetylacetone mono-*S*-methylisothiosemicarbazone according to mechanism **B** is by around 20 kJ/mol higher in comparison to that of methyl acetoacetate *S*-methylisothiosemicarbazone.

In Fig. 6, the free energy profiles for transformation of methyl acetoacetate *S*-methylisothiosemicarbazone and acetylacetone mono-*S*-methylisothiosemicarbazone according to both mechanisms **A** and **B** are depicted. In accordance with experimental results, methyl acetoacetate *S*-methylisothiosemicarbazone conforms to mechanism **B**. In this way, the system surmounts higher activation barriers, but acquires thermodynamically more stable product. On the other hand, acetylacetone mono-*S*-methylisothiosemicarbazone undergoes mechanism **A**. In this way, thermodynamically less stable product is yielded, but energetically very unfavorable step, i.e., elimination of bad leaving group, methane, is avoided. In other words, the reaction of methyl acetoacetate *S*-methylisothiosemicarbazone is thermodynamically controlled, whereas the reaction of acetylacetone mono-*S*-methylisothiosemicarbazone is kinetically controlled.

Conclusion

The reaction between *S*-methylisothiosemicarbazide hydrogen iodide and methyl acetoacetate proceeds by the formation of methyl acetoacetate *S*-methylisothiosemicarbazone. The exact structure of the final product was determined by 1D and 2D NMR spectroscopy and single-crystal X-ray diffraction analysis. The complete assignation of NMR data and positions of nitrogen atoms in the structure of the compound was performed by means of $^{1}H–^{15}N$ HSQC and $^{1}H–^{15}N$ HMBC spectra. The mechanism of transformation of methyl acetoacetate *S*-methylisothiosemicarbazone was elucidated by density functional theory, and compared to the previously reported mechanism of conversion of acetylacetone mono-*S*-methylisothiosemicarbazone into a 3-aminopyrazole derivative. It was concluded that the former reaction is thermodynamically controlled. In the case of the latter compound, the analogous mechanism would include elimination of bad leaving group, methane (in contrast to good leaving group, methanol), and because the reaction of acetylacetone mono-*S*-methylisothiosemicarbazone is kinetically controlled.

Experimental

Physical measurements

Melting point was determined on a Mel-Temp capillary melting points apparatus, model 1001 and is uncorrected. Elemental (C, H, N, S) analysis of the samples was carried out in the Center for Instrumental Analysis, Faculty of Chemistry, Belgrade. IR spectrum was recorded on a Perkin Elmer Spectrum One FT-IR spectrometer with a KBr disk, while HRMS analysis was performed on an Agilent MSD TOF mass spectrometer. ^{1}H- and ^{13}C NMR spectra were recorded on a Bruker Avance III 500 MHz spectrometer. The samples were recorded using $CDCl_3$ and DMSO-d_6. The full assignments of all reported NMR signals were made by use of 1D and 2D NMR experiments.

X-ray crystallography

Single crystal of the compound was glued on a glass fiber and mounted on a Gemini S diffractometer equipped using Sapphire3 CCD detector (Agilent Technologies). Sealed tube with Cu-target anode and graphite monochromator were used as source of X-radiation (Cu $K\alpha$, $\lambda = 1.5418$ Å). Data were collected with ω scan technique at room temperature. Reflection intensities were integrated and corrected for absorption (multi-scan) with CRYSALISPRO [26].

The structure was readily solved by direct methods using SIR92 [27]. The full-matrix least-squares refinement based on F^2 was performed with SHELXL-97 [28] integrated in SHELXLE graphical user interface [29]. All non-hydrogen atoms were refined anisotropically. Hydrogen atoms bonded to carbon atoms were introduced in idealized positions and refined as riding with U_{iso} fixed as 1.2 or $1.5U_{eq}$ of the parent atoms, while those bonded to nitrogen atoms were determined from ΔF map and refined isotropically. Hydrogen atoms belonging to the methyl group were found to occupy two equivalent sites and were refined as ideally disordered with 0.5 site occupancy factors. Crystallographic data are listed in Table S5 (Supplementary data). Molecular graphics was plotted with ORTEP-3 [30] and PLATON [31].

Crystallographic data for MOPC (**1**) have been deposited with the Cambridge Crystallographic Data Centre as Supplementary publication no. CCDC 902014. A copy of this data can be obtained, free of charge, via www.ccdc.cam.uk/data_request/cif, or by emailing data_request@ccdc.cam.ac.uk.

General procedure for the preparation of MOPC (**1**)

A mixture of thiosemicarbazide (3.00 g, 33.00 mmol) and methyl iodide (5.68 g, 40.00 mmol) in ethanol (15 mL)

was refluxed for 45 min. After cooling, white crystals of *S*-methylisothiosemicarbazide hydrogen iodide were filtered, washed with ethanol, and dried over $CaCl_2$. Yield: 5.91 g (76 %). A mixture of *S*-methylisothiosemicarbazide hydrogen iodide (2.80 g, 12.02 mmol), methyl acetoacetate (1.42 g, 12.26 mmol), and ethanol (9 mL) in a 50-mL round-bottomed flask was stirred for 1 h and left standing for 48 h at the room temperature. Afterward, the solvent was evaporated under reduced pressure giving *S*-methylisothiosemicarbazone (**2b**), which is used in the next step without further purification.

Spectral data for **2b**: ^{1}H NMR (500 MHz, $CDCl_3$): δ 2.27 (s, 3H), 2.69 (s, 3H), 3.39 (s, 2H); 3.75 (s, 3H); ^{13}C NMR (125 MHz, $CDCl_3$): δ 14.91, 19.61, 43.63, 52.31, 156.15, 168.76, 173.87.

After the solvent was evaporated, water (15 mL) was poured into the flask and the granulated NaOH (5.29 g, 13.22 mmol) was added immediately to the stirring mixture. The reaction heat was evolved and the external cooling was not applied. After 30 min of stirring, the mixture was left standing at the room temperature for 24 h. The formed enolate salt of pyrazol-5-one **16** was then filtered off, dried over $CaCl_2$. Yield: 1.05 g (54 %).

Spectral data for **16**: ^{1}H NMR (500 MHz, DMSO-d_6): δ 1.90 (s, 3H, CH_3), 4.37 (s, 1H, H at C4), 6.73 (d, 1H, $J = 4.0$ Hz, NH_2), 9.49 (d, 1H, $J = 4.0$ Hz, NH_2); ^{13}C NMR (125 MHz, DMSO-d_6): δ 15.03, 82.40, 151.09, 154.52, 166.28.

The compound **16** was treated with 2 M HCl with stirring. The solid was filtered off and dried over $CaCl_2$ giving the final compound MOPC (**1**). Yield: 0.68 g (75 %). The suitable single crystals of **1** for single-crystal X-ray diffraction analysis were obtained by recrystallization from methanol.

Spectral data for **1**: white powder; mp 175 °C; IR (KBr, cm^{-1}): 3309, 1708, 1643, 1556, 1386, 1350; ^{1}H NMR (500 MHz, DMSO-d_6): δ 2.11 (s, 3H, CH_3), 5.06 (s, 1H, H at C4), 7.68 (s, 1H, NH_2), 8.34 (s, 1H, NH_2), 12.21 (bs, 1H, NH); ^{13}C NMR (125 MHz, DMSO-d_6): δ 11.89 (CH_3), 90.96 (C4), 149.43 (C3), 150.45 (C=O), 163.35 (C5). Anal. Calcd. for $C_5H_7N_3O_2$ (141.13 g/mol): C, 42.55; H, 5.00; N, 29.77; Found: C, 42.39; H, 5.08; N, 29.50. HRMS (TOF, *m/z*) $[M + H]^+$, Calcd. for $C_5H_8N_3O_2$: 142.13740; Found: 142.06110.

Computational method

All calculations were carried out by the Gaussian 09 program [32]. To provide the compatibility of the results of the present investigation with those presented in our previous paper [12], the calculations were performed at the B3LYP/6-311++G(d,p) level of theory [33–35]. Geometry optimizations for all species under investigation were achieved for the aqueous phase without any symmetry constraints. The influence of water as solvent ($\varepsilon = 78.36$) was estimated by the conductor-like solvation model (CPCM) [36, 37].

TSs were searched by synchronous transit guided quasi-Newton method [38]. The intrinsic reaction coordinates, from the TSs down to the two lower energy structures, were traced by the IRC routine in Gaussian to verify that each saddle point is linked with corresponding reactant complex (RC) and product complex (PC). The structure of RC for each elementary reaction was obtained in the following way: the geometry which first results from progression backward along the reaction coordinate starting from the TS was selected, and fully optimized without any movement restriction. Similarly, the structure of PC for each elementary reaction was determined by selecting the geometry which first results from progression forward along the reaction coordinate, and reoptimizing the selected geometry. The obtained geometries were verified, by normal mode analysis, to be minima (no imaginary frequencies) or maxima on the potential energy surface (one imaginary frequency). NBO analysis [39] was performed for all species.

Acknowledgments The authors are grateful to the Ministry of Education, Science and Technological Development of the Republic of Serbia for financial support (Grant No. 172016).

References

1. Brogden RN (1986) Drugs 32:60–70
2. Chandrasekharan NV, Dai H, Roos KLT, Evanson NK, Tomsik J, Elton TS, Simmons DL (2002) Proc Natl Acad Sci USA 99:13926–13931
3. Watanabe T, Tahara M, Todo S (2008) Cardiovasc Ther 26:101–114
4. Kimata A, Nakagawa H, Ohyama R, Fukuuchi T, Ohta S, Suzuki T, Miyata N (2007) J Med Chem 50:5053–5056
5. Kakiuchi Y, Sasaki N, Satoh-Masuoka M, Murofushi H, Murakami-Murofushi K (2004) Biochem Biophys Res Commun 320:1351–1358
6. Brana MF, Gradillas A, Ovalles AG, López B, Acero N, Llinares F, Muñoz Mingarro D (2006) Bioorg Med Chem 14:9–16
7. Tripathy R, Ghose A, Singh J, Bacon ER, Angeles TS, Yang SX, Albom MS, Aimone LD, Herman JL, Mallamo JP (2007) Bioorg Med Chem Lett 17:1793–1798
8. Rajendran G (1999) Asian J Chem 11:153–161
9. Pal S, Mareddy J, Devi NS (2008) J Braz Chem Soc 19: 1207–1214
10. Katritzky AR, Barczynski P, Ostercamp DL (1987) J Chem Soc Perkin Trans 2:969–975
11. Fox MA, Whitesell JK (2004) Nucleophilic addition and substitution at carbonyl group, organic chemistry, 3rd edn. Jones and Bartlett Publishers, Boston
12. Marković S, Joksović MD, Bombicz P, Leovac VM, Marković V, Joksović Lj (2010) Tetrahedron 66:6205–6211
13. Llamas-Saiz AL, Foces-Foces C, Elguero J (1994) J Mol Struct 319:231–260

14. Allen FH, Kennard O, Watson DG, Brammer L, Orpen AG, Taylor R (1987) J Chem Soc Perkin Trans 2:S1–S19
15. Casas JS, Castaño MV, Castellano EE, García-Tasende MS, Sánchez A, Sanjuán ML, Sordo J (2000) Eur J Inorg Chem 83–89:2–9
16. Casas JS, Castellano EE, Ellena J, García-Tasende MS, Sánchez A, Sordo J, Touceda A, Rodríguez SV (2007) Polyhedron 26:4228–4238
17. Duan X-M, Fan M-L, Zheng P-W, Li J-S, Huang PM (2006) Acta Crystallogr E 62:o2019
18. Sieler J, Kempe R, Hennig L, Becher J (1992) Z Kristallogr 198:313–314
19. Lorenzotti A, Marchetti F, Pettinari C, Pettinari R, Skelton BW, White AH (2005) Inorg Chim Acta 358:3190–3200
20. Aleksanyan MS, Karapetyan AA, Oganisyan ASh, Struchkov YuT (1997) J Struct Chem 38:989–992
21. Wang Q, Zhang Y, Wang R, Yang Y-L, Zhi F (2008) Acta Crystallogr E 64:o1924
22. Foces-Foces C, Fontenas C, Elguero J, Sobrados I (1997) An Quim 93:219
23. Etter MC (1990) Acc Chem Res 23:120–126
24. Desiraju G (1995) Angew Chem Int Ed 34:2311–2327
25. Allen FH, Baalham CA, Lommerse JPM, Raithby PR (1998) Acta Crystallogr B 54:320–329
26. CrysAlisPro Software system, Version 1.171.35.19. Agilent Technologies UK Ltd., Oxford
27. Altomare A, Cascarano G, Giacovazzo C, Gualardi A (1993) J Appl Crystallogr 26:343–350
28. Sheldrick GM (2008) Acta Crystallogr A 64:112–122
29. Hübschle CB, Sheldrick GM, Dittrich B (2011) J Appl Crystallogr 44:1281–1284
30. Farrugia LJ (1997) J Appl Crystallogr 30:565
31. Spek AL (2009) Acta Crystallogr D 65:148–155
32. Frisch MJ, Trucks GW, Schlegel HB, Scuseria GE, Robb MA, Cheeseman JR, Scalmani G, Barone V, Mennucci B, Petersson GA, Nakatsuji H, Caricato M, Li X, Hratchian HP, Izmaylov AF, Bloino J, Zheng G, Sonnenberg JL, Hada M, Ehara M, Toyota K, Fukuda R, Hasegawa J, Ishida M, Nakajima T, Honda Y, Kitao O, Nakai H, Vreven T, Montgomery JA Jr, Peralta JE, Ogliaro F, Bearpark M, Heyd JJ, Brothers E, Kudin KN, Staroverov VN, Kobayashi R, Normand J, Raghavachari K, Rendell A, Burant JC, Iyengar SS, Tomasi J, Cossi M, Rega N, Millam JM, Klene M, Knox JE, Cross JB, Bakken V, Adamo C, Jaramillo J, Gomperts R, Stratmann RE, Yazyev O, Austin AJ, Cammi R, Pomelli C, Ochterski JW, Martin RL, Morokuma K, Zakrzewski VG, Voth GA, Salvador P, Dannenberg JJ, Dapprich S, Daniels AD, Farkas O, Foresman JB, Ortiz JV, Cioslowski J, Fox DJ (2009) Gaussian 09, Rev A1. Gaussian, Wallingford
33. Becke AD (1988) Phys Rev A 38:3098–3100
34. Lee C, Yang W, Parr RG (1988) Phys Rev B 37:785–789
35. Becke AD (1993) J Chem Phys 98:5648–5652
36. Barone V, Cossi M (1998) J Phys Chem A 102:1995–2001
37. Cossi M, Rega N, Scalmani G, Barone V (2003) J Comput Chem 24:669–681
38. Peng C, Ayala PY, Schlegel HB, Frisch MJ (1996) J Comput Chem 17:49–56
39. Foster JP, Weinhold F (1980) J Am Chem Soc 102:7211–7218